Journal of Power Sources 184 (2008) 29–37

Contents lists available at ScienceDirect

Journal of Power Sources

journal homepage: www.elsevier.com/locate/jpowsour

Characterisation of porous carbon electrode materials used in proton exchange membrane fuel cells via gas adsorption

M.J. Watt-Smith[a,b], S.P. Rigby[b], T.R. Ralph[a,c], F.C. Walsh[a,*]

[a] Electrochemical Engineering Laboratory, Energy Technology Research Group, School of Engineering Sciences, University of Southampton, Highfield, Southampton SO17 1BJ, United Kingdom
[b] Department of Chemical Engineering, University of Bath, Claverton Down, Bath BA2 7AY, United Kingdom
[c] Johnson Matthey Fuel Cells, Great Western Way, Swindon SN5 8AT, United Kingdom

ARTICLE INFO

Article history:
Received 2 October 2007
Received in revised form 27 May 2008
Accepted 8 June 2008
Available online 14 June 2008

Keywords:
Electrode materials
Fractal dimension
Gas adsorption
PEM fuel cell
Surface area
Structural models

ABSTRACT

Porous carbon materials are typically used in both the substrate (typically carbon paper) and the electrocatalyst supports (often platinised carbon) within proton exchange membrane fuel cells. Gravimetric nitrogen adsorption has been studied at a carbon paper substrate, two different Pt-loaded carbon paper electrodes and three particulate carbon blacks. N_2 BET surface areas and surface fractal dimensions were determined using the fractal BET and Frenkel–Halsey–Hill models for all but one of the materials studied. The fractal dimensions of the carbon blacks obtained from gas adsorption were compared with those obtained independently by small angle X-ray scattering and showed good agreement. Density functional theory was used to characterise one of the carbon blacks, as the standard BET model was not applicable.

1. Introduction

The varieties of carbon [1] include activated carbon, carbon black, carbon fibres and carbon cloth, with clear definitions of these and all the forms of carbon as a solid described by Fitzer et al. [2]. In most catalytic applications, including proton exchange membrane (PEM) fuel cells [3], carbon-containing composites are the substrates under consideration. Carbon paper is often chosen as the substrate in PEM fuel cells and is usually prepared from the random weaving of carbon fibres, with the extent and nature of the surface area and porosity being dependent upon the precursor material and its manufacturing history.

Carbon blacks are often used as the support material for precious metal electrocatalyst coatings. Carbon blacks play a major role in structural components, conductive supports, and electrocatalysts in batteries and fuel cells. Such materials possess a relatively high surface area which is derived from the fine particle size of the material, rather than from porosity. Optimising the structural properties of carbon blacks is an important area of research due to their importance in fuel cell applications.

The characterisation of carbon blacks has previously been determined using a comparison of nitrogen and carbon dioxide adsorption at 77 and 298 K, respectively [4], atomic force microscopy [5], Raman and neutron scattering [6], X-ray diffraction [7], small angle X-ray scattering (SAXS) [8], transmission electron microscopy and small angle neutron scattering [9]. Xu et al. [10] used various gas adsorbates to investigate the structural properties of different grades of carbon blacks. Analysis of the data using the work of Pfeifer and Avnir [11] and Halsey [12] determined the fractal dimension of the materials.

Carbon fibre materials tend to have carbon content greater than 90%. Since the final carbon fibres contain almost 100% carbon, any fibrous material with a carbon backbone can potentially be used as a precursor which would yield a carbonaceous residue. Rayon and polyacrylonitrile are precursors for many of the commercial fibres that are produced, although other precursors such as pitch (a by-product of the petroleum or coal-coking industry), phenolic resins and polyacetylenes have also been used [13]. Gas adsorption is a common technique in the study of structural properties of carbon fibres; a review by Do and Do [14] has considered the adsorption of supercritical fluids (Kr, Ar, N and CH_4) on different porous and non-porous carbons. Studies using Kr [15–17] and N_2 [18,19] have also been performed. Techniques such as scanning electron microscopy and atomic force microscopy [20], X-ray diffraction and Raman spectroscopy [21], scanning tunnelling microscopy [22,23]

* Corresponding author. Tel.: +44 23 8059 8752.
E-mail address: F.C.Walsh@soton.ac.uk (F.C. Walsh).

0378-7753/$ – see front matter © 2008 Elsevier B.V. All rights reserved.
doi:10.1016/j.jpowsour.2008.06.015

Nomenclature

C	BET constant
d	fractal dimension
E_i	energy of adsorption
E_L	liquefication energy
n	amount of gas adsorbed (mol)
n_m	molecular capacity
N_A	Avagadro constant (6.023×10^{23} mol^{-1})
P	applied pressure (bar)
P_0	saturation pressure (bar)
R	molar gas constant (8.314 J mol^{-1} K^{-1})
T	temperature (K)
V	volume of gas adsorbed at equilibrium pressure (m^3)
V_m	volume of gas in monolayer (m^3)

Greek letter

σ	molecular cross-sectional area (nm^2)

and SAXS [24] have been used to investigate the structure and physical properties of carbon fibres.

The work presented here aims to interpret isothermal data, using a selection of established models, for a variety of important carbon materials that are typically and routinely used in PEM fuel cells. The materials include a carbon paper substrate for electrocatalysts and also two Pt-loaded electrodes. In addition, three carbon blacks, which are used as the electrocatalyst support, are examined. The results aim to give a quantitative and accurate description of the structural properties of these materials. Both classical and recently developed adsorption models are considered and the paper represents an ambitious attempt to fit these models to standard isotherms of practical PEM fuel cell carbons. Features of this paper include: (a) a quantitative consideration of several adsorption models, (b) classical adsorption models are complemented by modern, (e.g., modified fractal) ones, (c) adsorption data on carbon materials in the paper have not previously been reported, (d) not all of the materials can be fitted to simple adsorption models and (e) problems in applying adsorption models to certain carbons are highlighted.

2. Theory

2.1. Determination of surface area—the BET method

2.1.1. The BET model

The most popular technique for the determination of the surface area over a wide range of porous materials (the BET model) is the method proposed by Brunauer et al. [25]. According to the BET model, the molecules in one layer can act as possible sites for the adsorption of molecules in the next layer. When the rate of condensation (adsorption) is equal to the rate of evaporation (desorption), an equilibrium pressure, P, is achieved at a given temperature, T. For adsorption in each layer, the following expression applies:

$$a_i P \theta_{i-1} = b_i \theta_i \ \exp\left(-\frac{E_i}{RT}\right) \tag{1}$$

where θ_{i-1} and θ_i are, respectively, the fractions of surface covered by the $i-1$ and i layers, a_i and b_i are adsorption and desorption constants and E_i is the energy of adsorption for the ith layer. Each layer has a different set of values of a_i, b_i and E_i but it is assumed that for all layers after the first, these parameters remain constant and also that $E_i = E_L$, the liquefaction energy. Also, the assumption is made that E_i is not dependent on surface coverage, θ_i. This implies both a uniform array of surface sites and the absence of lateral interactions between the adsorbed molecules. A further assumption is made to the model, which is that the multilayer has an infinite thickness at $P/P_0 = 1$. This assumption allows the simplification of the summation of the amounts adsorbed in all layers and allowed the production of the BET equation:

$$\frac{P/P_0}{n(1-P/P_0)} = \frac{1}{n_m c} + \frac{C-1}{n_m c}\frac{P}{P_0} \tag{2}$$

where n_m is the monolayer capacity and C is an empirical constant.

According to the BET theory, the constant C is related exponentially to E_1 by the simplified equation:

$$C \approx \exp\left[\frac{E_1 - E_L}{RT}\right] \tag{3}$$

where the quantity $E_1 - E_L$ is termed the net molar energy of adsorption. The value of C is an indication of the adsorbent–adsorbate interactions, with high values ($C > 100$) indicative of high interaction strengths, whilst medium (<80) and low values (<20) represent medium and low interaction strengths.

The validity of the original BET equation is always confined to a limited part of the isotherm, which is seldom above $P/P_0 = 0.3$. The BET model does not take into account lateral interactions between the adsorbed molecules in the first layer, and assumes that all higher layers have liquid-like properties. Another prerequisite of the model is that the surface sites are all equivalent (i.e. a uniform surface) and that the surface is flat. Although the BET method includes assumptions and limitations, it is widely used for the evaluation of the surface area from physisorption isotherm data.

2.1.2. Determination of surface area

Two stages are involved in the evaluation of the surface area. Firstly, it is necessary to construct the BET plot and to derive a value of n_m. The next stage is the calculation of the specific surface area, a(BET), which requires knowledge of the average area, σ, occupied by each molecule in the completed monolayer. The value of n_m and C can be solved by plotting $(P/P_0)/[n(1-P/P_0)]$ against P/P_0. The usual range of linearity of the BET plot is $0.1 < P/P_0 < 0.3$. This range varies, depending on the material investigated. Sufficient experimental points on the adsorption isotherm must be determined to select the region providing the best linear fit. The second stage in the application of the BET method is the calculation of the specific surface area, a(BET), from the monolayer capacity n_m:

$$\alpha(\mathrm{BET}) = n_m N_A \ \sigma \tag{4}$$

where N_A is the Avagadro constant (6.023×10^{23} mol^{-1}) and σ is the average area occupied by each adsorbed molecule in the completed monolayer. Varied values of σ are found in the literature; the value of σ is, to some extent, dependent on the adsorbent-adsorptive system and temperature and not just on the adsorbate. If the adsorbent–adsorbate interactions are strong and the temperature is low, the monolayer is likely to be localised and, under these conditions, the monolayer structure tends to be controlled by surface chemistry.

The most widely used adsorptive for surface area determination is nitrogen (at 77 K) as it is considered to be the most suitable adsorptive for the determination of the surface area of nonporous, macroporous, or mesoporous solids. It is assumed that the BET nitrogen monolayer is close-packed, giving a $\sigma(N_2) = 0.162$ nm^2 at 77 K [26].

2.2. Fractal analysis

The concept of fractality and the definition of the fractal dimension are related to the nature of the measurements of the surface area and other geometrical parameters of porous solids. The fractal approach provides a method of evaluating the absolute area of a finely divided or porous solid.

The fractal dimension is a structural parameter that quantifies the scaling invariance of self-similar systems [27]. If an object can be decomposed into λ similar parts of size n times smaller than the whole, the fractal dimension is defined as a scaling exponent in the relation between the fragmentation parameter λ and the contraction ratio, n:

$$\lambda = n^d \tag{5}$$

The fractal dimension of self-similar objects can be determined by different methods. In the method of "box counting", the fractal is covered by equal boxes of size a. The number of boxes, N depends on the box size a, and the volume V occupied by the boxes and scales as:

$$V(a) \propto a^{3-d} \tag{6}$$

The method of molecular tiling was introduced by Pfeifer and Avnir [11] and involves a comparison of the monolayer capacities of different adsorbates. The molecules of different sizes are used as 'gauges' to determine the surface area of an adsorbent. In a standard adsorption experiment, the surface area, S, is estimated as the product of the number of molecules in the monolayer capacity n_m and the effective area occupied by one molecule, σ:

$$S = n_m \sigma \tag{7}$$

According to the method of tiling, the number of 'gauges' needed to cover a fractal surface scale with the linear size of the gauges, $a = \sigma^{1/2}$ and:

$$n_m = n_{m0}\left(\frac{\sigma}{\sigma_0}\right)^{d/2} \tag{8}$$

where the subscript '0' denotes the adsorbate taken as a reference. The fractal dimension, d, can be determined from a set of adsorption measurements using different adsorbates. The monolayer capacity is calculated from the gas adsorption isotherm using the BET method, as mentioned earlier. A problem of using the method of molecular tiling is the limited range of length-scales available for fractal analysis. The method can reveal information about the molecular scale roughness of the adsorbent surface but it is difficult to make conclusions about the fractality, which implies a hierarchical structure over a wide range of scales.

Pfeifer et al. [28,29] adopted the Frenkel–Halsey–Hill (FHH) [12] equation for multilayer adsorption of fractal surfaces. The method is based on an expression for the surface fractal dimension from an analysis of multilayer adsorption on a fractal surface, such that:

$$\ln\left(\frac{V}{V_m}\right) = C + S\ \ln\left[\ln\left(\frac{P_0}{P}\right)\right] \tag{9}$$

where V is the volume of gas adsorbed at equilibrium pressure P, V_m is the volume of gas in a monolayer, and P_0 is the saturation pressure. The constant C is a pre-exponential factor, and S is a power law exponent dependent on d, the surface fractal dimension and the mechanism of adsorption. There are two limiting cases for the model. At the lower end of the isotherm, which represents the early stages of multilayer build-up, the film/gas interface is controlled by attractive van der Waal's forces between the gas and the solid. This tends to allow the film/gas interface to replicate the surface roughness. The value of the constant, S is given by:

$$S = \frac{d-3}{3} \tag{10}$$

When there is a high degree of coverage, however, the interface is determined by the liquid/gas surface tension which causes the interface to move further away from the surface and reduces the surface area. In this case, S is given by:

$$S = d - 3 \tag{11}$$

The surface fractal dimension, d may physically take values in the range $2 \le d \le 3$, with a value of 2 indicating a perfectly smooth surface, whilst a value of 3 is indicative of a highly disordered surface. An alternative analysis method to derive surface fractal dimensions from gas adsorption data is to use the fractal version of the BET theory. The concept is based upon the fact that, for a fractal surface, the area available for adsorption in the ith layer of adsorptive decreases by the factor f_i and is given by:

$$f_i = \frac{A_i}{A_1} = i^{\alpha-1} \tag{12}$$

where $\alpha = 3 - d$. Mahnke and Mögel [30] suggested an alternative expression to the fractal BET equation initially proposed by Fripiat et al. [31]:

$$\log[V_{(P/P_0)}] = \log(V_m) + \log\left[\frac{C(P/P_0)}{1-(P/P_0)+C(P/P_0)}\right] - \alpha\ \log[1-(P/P_0)] \tag{13}$$

where C is the BET constant. Mahnke and Mögel [30] suggested that the following procedure should be performed to obtain a value for α: (a) estimate C and V_m from the BET [25] equation then (b) evaluate the plot of:

$$\log\left[\frac{V}{V_m}\frac{1-(P/P_0)+C(P/P_0)}{C(P/P_0)}\right] (= \log(Z)) \quad vs. \quad -\log[1-(P/P_0)] \tag{14}$$

The plot should be linear and the slope provides an estimate for $\alpha = 3 - d$.

It has previously been shown [32] that adsorption of different adsorbates on heterogeneous surfaces may vary due to interaction strength differences between the adsorbate and adsorbent. In a similar way, if a surface is composed of multiple components, these interaction strength differences may also occur. This can be investigated by using a two-component BET model [32]:

$$\frac{V}{V_m} = \frac{P/P_0}{1-(P/P_0)^{3-d}}\left[\frac{\theta C_1}{1+(C_1-1)(P/P_0)} + \frac{(1-\theta)C_2}{1+(C_2-1)(P/P_0)}\right] \tag{15}$$

The overall isotherm is thus a composite of two BET-type equations, each one corresponding to the two types of surface patches. C_1 and C_2 are the BET constants for surface patches of types 1 and 2, respectively, d is the surface fractal dimension and θ is the fraction of the surface occupied by patches of type 1. This approach may highlight the differences in strength of interaction between the adsorbed nitrogen and the carbon blacks and Pt within the fuel cell electrodes.

2.3. Small angle X-ray scattering

Small-angle X-ray scattering (SAXS) is a technique that allows the determination of the particle size distribution and the measurement of the specific surface area. A beam of X-rays is scattered

by the electrons in an irradiated material. As the distribution of electrons throughout a material is heterogeneous, fluctuations in electron density (number of electrons per unit volume) exist at different zones within the sample. When the dimensions of these spatial inhomogeneities are similar to the wavelength of the incident X-ray beam, λ then most of the scattering is observed at angles greater than 10°. However, if the inhomogeneities in the electron density extend over the distances in the range between ca. 0.5 and 400 nm, then the intensity of scattered X-rays is appreciable at small angles. The SAXS technique can be used to provide information on structures much larger than the normal inter-atomic distances encountered in dense materials.

Porous materials greatly scatter X-ray radiation near the X-ray beam, due to the system of volume-distributed local inhomogeneities of electron density (submicropores and micropores). Pore sizes and shapes, exceeding the wavelength of X-ray radiation, condition the angular range of such scattering and the scattering intensity, $I(q)$ is mainly determined by pore concentration and electron density gradient at the pore-matrix border.

The surface roughness on a scale in the range of the inverse of q covered in the SAXS measurements can be determined [33]. This is achieved by describing the material as having surface fractal properties, and a decay in the scattered intensity $I(q)$ is given by:

$$I(q) \sim q^{-(6-d)} \tag{16}$$

where d is the surface fractal dimension. Typically, values of $2 < d < 3$ occur, with $d = 2$ representing a smooth surface, whilst $d = 3$ is indicative of a highly disordered surface. The surface fractal dimension obtained from SAXS can also be used as the basis to obtain, independently of gas adsorption, an estimate of the specific surface area, as perceived by a given adsorbate, of a porous solid with a fractally rough internal surface. If the porous solid consists of a close-packing of spherical particles of radius R, which each possess a fractally rough surface of dimension d, then the specific surface area of the solid (A_s) as perceived by a particular adsorbate species is given by:

$$A_s = \frac{3r^2(R/r)^d}{R^3\rho_s} \tag{17}$$

where r^2 is the cross-sectional area of a close-packed adsorbate molecule and ρ_s is the skeletal mass density of the solid. For porous solids consisting of packed particles, the characteristic particle size (R) can be obtained using electron microscopy [33], mercury porosimetry [34] or SAXS [35].

3. Experimental details

The carbon materials examined in this work include those conventionally used within a membrane electrode assembly (MEA) in a PEM fuel cell. Three types of carbon paper were examined, namely (i) an unloaded (denoted CU1), (ii) a low Pt-loading (0.39 mg cm^{-2}, denoted CL1) and (iii) a high Pt-loading (4.7 mg cm^{-2}, denoted CH1). The PEM fuel cell electrodes consisted of a carbon paper substrate and a mixture of activated carbon and Pt as the support and catalyst, respectively. Electrode materials were supplied by Johnson Matthey Technology Centre. Both CH1 and CL1 were supported by TGP-H-060 Toray paper. The catalyst layer of CL1 was made up of 40 wt% Pt supported on Vulcan XC72R containing 75 wt% Nafion® 1100 EW ionomer (based on carbon weight) at a loading of 0.39 mg Pt cm^{-2}. The catalyst layer of CH1 was made of Pt black containing 6 wt% Teflon at 4.4 mg Pt cm^{-2}. Both samples also had a top coat of Nafion® ion exchange resin at a loading of 0.5 mg Pt cm^{-2}.

Three types of particulate carbon used as a Pt support material, were also examined. These included (1) a conductive carbon, (2) Vulcan XC72R and (3) an acetylene black (denoted CP1, CP2 and CP3, respectively). The structural and physical characteristics of the materials were not known prior to analysis.

3.1. Experimental methods

3.1.1. Scanning electron microscopy

Scanning electron micrographs were obtained for the carbon paper samples (CU1, CL1 and CH1) using a JEOL JSM-6310 microscope. The samples were cut, using a clean steel scalpel blade, into 0.5 cm^2 squares and fixed to an aluminium sample dish using a conductive carbon tape. The imaging was conducted at an operating voltage of 15 kV. Images were acquired and stored directly to a PC using the image capture software Semafore version 4. Multiple samples of the same batch were examined to investigate structural heterogeneity.

3.1.2. Nitrogen adsorption

Nitrogen adsorption experiments were performed at 77 K using a Micromeritics accelerated surface area and porosimetry (ASAP) 2010 apparatus. Carbon paper samples were cut with a clean scalpel blade into 50 strips, each having dimensions of 0.7 cm × 2 cm. The number of strips was kept constant in all experiments. The sample (collection of 50 strips) was then placed into a pre-weighed round-bottomed glass tube and a glass spacer was placed gently into the sample tube to reduce the free-space volume. A sealing frit was then fitted to the opening of the tube so as to seal the tube after degassing prior to analysis. The sample tube and its contents were then loaded into the degassing port of the apparatus. A heating jacket was applied to the tube and the sample was heated, under vacuum, to 100 °C for 24 h.

The purpose of the thermal pre-treatment for each sample was to drive off any physisorbed water on the sample whilst leaving the morphology of the sample unchanged. Once the preparation was completed, the heating jacket was removed and the sample was allowed to cool down to room temperature (295 K). The sample tube and its contents were then re-weighed to obtain the dry weight of the sample, which was entered into the necessary section of the software program, prior to transfer of the sample tube to the analysis port for the automated analysis procedure.

The sample tube was immersed in liquid nitrogen at 77 K before the adsorption measurements were taken in the relative pressure region of 0.05–1.00 P/P_0. The software controlling the automated apparatus performed a leak-checking procedure and an equilibration time of 45 s was used for each adsorption point. Once the experiment was completed, the data values of the adsorption/desorption isotherms were available for analysis. The cross-sectional area of nitrogen, σ, was taken to be 0.162 nm^2. The same procedure was used for the carbon black materials, the nominal amount of each sample analysed being 250 mg.

3.1.3. Small angle X-ray scattering

SAXS patterns were run on the carbon black samples (CP1–CP3) using the DUBBLE SAXS beamline on BM26B at the European Synchrotron Radiation Facility (ESRF). The two-dimensional patterns were corrected for detector efficiency and calibrated against silver behenate and pixels at the same radius were averaged to produce one-dimensional patterns.

3.1.4. Transmission electron microscopy

Transmission electron micrographs of the carbon paper samples (CU1, CL1 and CH1) were obtained using a Jeol 1200 microscope. The samples were embedded in a spurr's resin and vacuum-treated to enhance resin penetration and to ensure that the samples were degassed. The samples were sectioned using a microtome and

freshly prepared glass knives. Images were acquired using a 35 mm SLR camera, the negatives being digitized for analysis.

4. Results and discussion

4.1. Carbon paper samples CU1–CH1

Fig. 1 shows a series of scanning electron micrograph (SEM) images of the carbon paper electrodes investigated in this work. Fig. 1(a) is a micrograph of CH1 and is comprised of a series of interwoven and overlapping carbon fibres, with typical diameters over the range of 5–15 μm. A micrograph of an individual fibre is shown in Fig. 1(b) and illustrates the 'plate-like' structure of the fibre together with the presence of grooves along the axial dimension. Fig. 1(a) shows that the carbon substrate does not possess pores, as defined in the conventional sense but open areas; 'holes' exist between the overlapping fibres. These holes vary in size from ca. 10 to 100 μm, whilst Fig. 1(b) implies that the individual fibres have limited or zero porosity themselves (based on the scales accessible by electron microscopy).

Fig. 1(c) and (d) are SEM images of the carbon substrate loaded with 0.39 mg Pt cm^{-2} (denoted CL1). Fig. 1(c) shows how the surface of CL1 consists of irregular-shaped 'packets' of deposited Pt, with large cracks seen between the individual packets. It can be further seen in Fig. 1(c) that small imperfections in the Pt layer have caused small holes and larger agglomerates randomly positioned within the surface. Fig. 1(c) and (d) illustrates a certain degree of heterogeneity in terms of surface deposition and coverage. This heterogeneity is obtained due to the larger overall volume of the catalyst used in the preparation of the electrode. Fig. 1(d) shows an individual fibre that is coated in Pt and is at a considerable depth within the paper (relative to the overall thickness of the paper). This sample is typically used as an electrode in a MEA and the purpose of the Pt layer is to catalyse the oxidation of hydrogen or the reduction of oxygen. If the Pt layer does not cover the substrate effectively, the catalytic activity of the electrode decreases; the performance of the electrode assembly is then lower.

Fig. 1(e) shows a SEM micrograph of sample CH1. The Pt loading of CH1 is over 10 times greater than CL1, as its typical application is in membrane electrode assemblies that require a high current density together with a long service lifetime. Fig. 1(e) clearly shows that the deposition of Pt is not uniform, and that areas with none or little Pt are present. This electrode has a thinner layer of catalyst (platinum black) due to the absence of a carbon support. This fact results in a lower volume of material available to coat the carbon fibre substrate. Fig. 1(f) shows the nodular arrangement of the Pt-activated C agglomerates, which range from ca. 10 to 100 nm in size and qualitatively imply a higher surface area than sample CL1.

Fig. 2 shows a series of transmission electron micrographs (TEMs) of the carbon paper samples investigated. Fig. 2(a) is a TEM micrograph of an individual fibre from sample CU1, and very clearly illustrates the plate-like formation of the carbon structure. The TEMs suggest a limited degree of porosity is present with any available porosity only accessible between the plates themselves.

TEMs for sample CL1 are shown in Fig. 2(b) and (c). Fig. 2(b) shows two open, elliptical regions in the top-right and bottom-left of the image and can be attributed to two individual fibres. The majority of the features seen in Fig. 2(b) are the activated carbon and Pt mixture that serves as the porous support and electrocatalyst, respectively. Fig. 2(c) is a high-resolution image focussing on the activated carbon and Pt particles. The idealised structure for the support [36] is envisaged as large carbon agglomerates supporting a highly dispersed level of a low concentration of Pt. The darkened areas of Fig. 2(c) are the activated carbon support, whilst the lighter more dispersed and smaller parts, being the Pt catalyst.

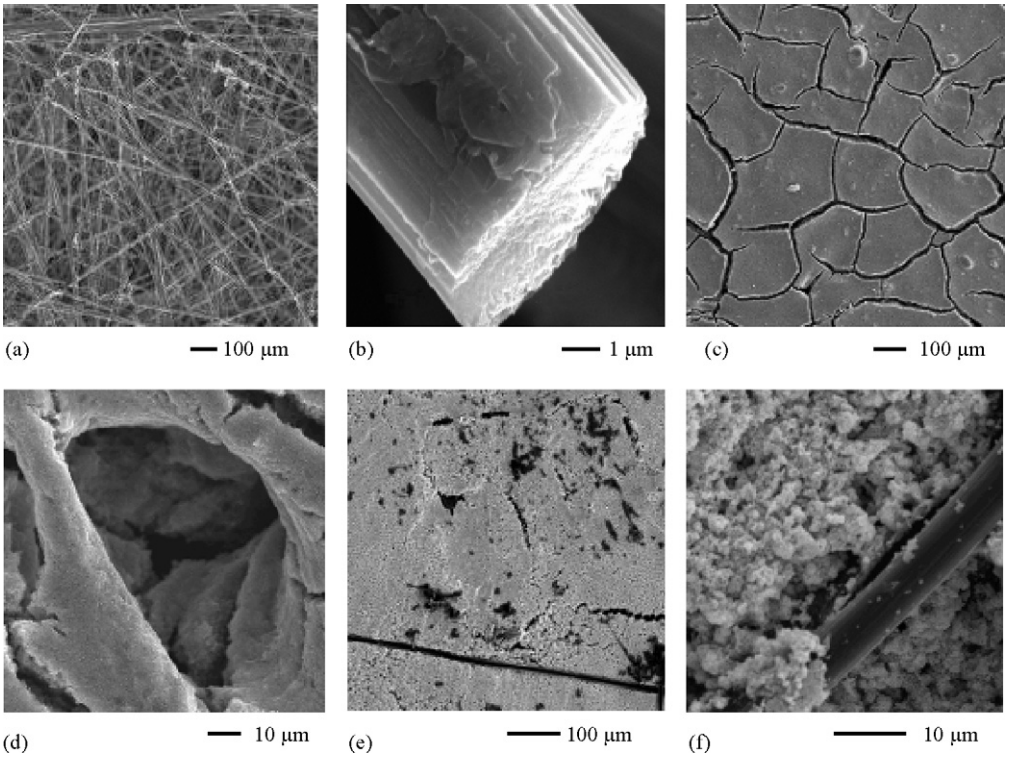

Fig. 1. Scanning electron micrographs of the carbon paper materials investigated (a) teflonated carbon substrate (sample CU1), (b) individual carbon fibre (sample CU1), (c) carbon paper with a loading of 0.39 mg Pt cm^{-2} (sample CL1), (d) increased magnification of carbon paper with 0.39 mg Pt cm^{-2} (sample CL1), (e) carbon paper with 4.7 mg Pt cm^{-2} (sample CH1), (f) increased magnification of carbon paper with 4.6 mg Pt cm^{-2} (sample CH1).

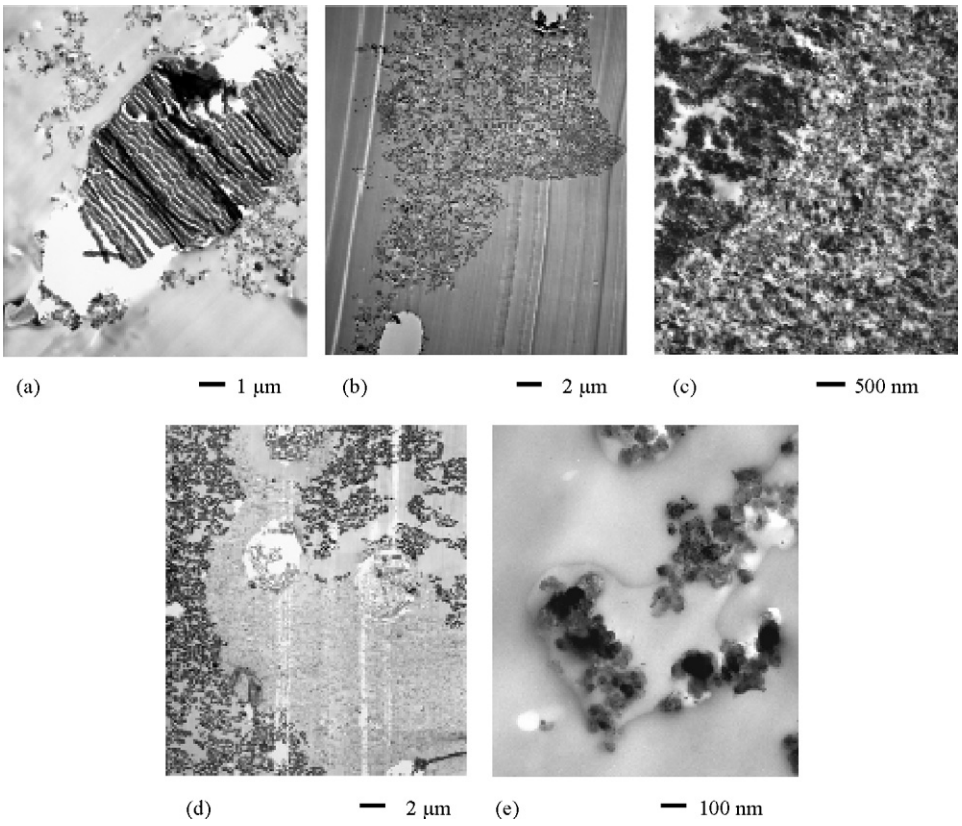

Fig. 2. Transmission electron micrographs of particulate carbon samples: (a) an individual fibre from unloaded sample CU1; (b) and (c) low loaded (0.39 mg cm^{-2} Pt) sample CL1, (d) and (e) high loaded (4.7 mg cm^{-2} Pt) sample CH1.

TEMs of sample CH1 are shown in Fig. 2(d) and (e). Individual fibres, shown by the round areas within the middle of Fig. 2(d) are similar to that seen in Fig. 2(b). The light grey area is the resin used to set the sample, whilst the dark black areas are the carbon–Pt mixture. This can be seen more clearly in Fig. 2(e), with the lighter areas representing an area of the carbon–Pt mixture that contains a higher level of Pt, compared to the darker areas of carbon containing less Pt.

The isotherms for the adsorption of nitrogen on samples CU1, CL1 and CH1 are shown in Fig. 3. The isotherms are all typical of a type II response, although the amounts adsorbed are very low. Type II isotherms are usually the result of monolayer–multilayer adsorption on the open surface of a nonporous or macroporous adsorbent. However, due to the low amounts adsorbed, it can be inferred that the structures are relatively non-porous, or show very limited porosity.

Sample CL1, which has a lower loading of Pt cm^{-2}, adsorbed a greater amount than CH1. This implies that the surface roughness (and hence surface area) is greater with a lower loading of Pt when these two samples are compared. Fits of the data to the fractal FHH model [11] and fractal BET model [30] are shown in Figs. 4 and 5.

Table 1 illustrates the parameters obtained from the fits of the data of samples CU1, CL1 and CH1 to the BET [25], fractal FHH [11] and fractal BET [30] models. It can immediately be seen that the surface areas obtained are all low, with sample CL1 showing the highest. The fractal dimensions obtained from both the fractal FHH [11] and fractal BET [30] model follow a similar trend. The fractal dimension for CU1 is higher than that for CL1 and CH1. The fractal

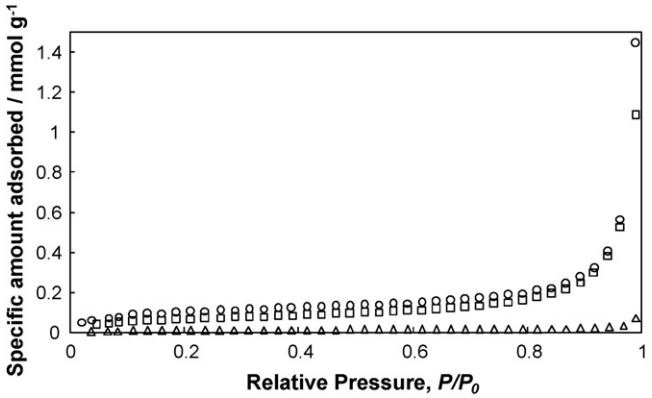

Fig. 3. Nitrogen adsorption isotherms for carbon paper samples CU1 (△), CL1 (○) and CH1 (□).

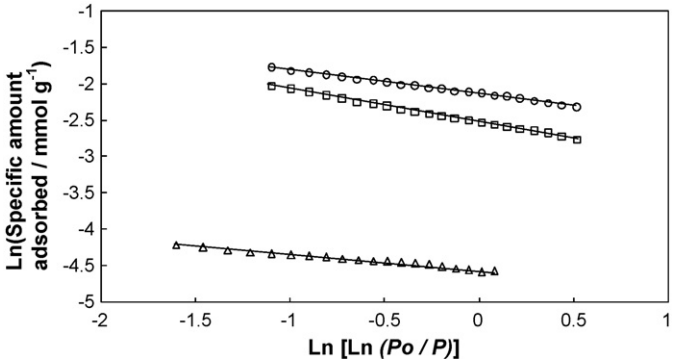

Fig. 4. Examples of typical fits (solid lines) to the fractal FHH [11] model to nitrogen adsorption isotherms for carbon paper samples CU1 (△), CL1 (○) and CH1 (□).

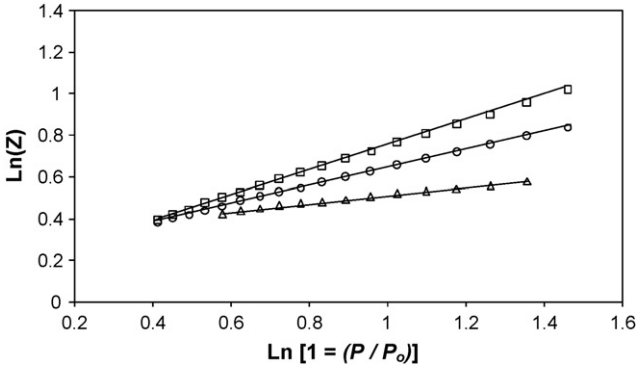

Fig. 5. Examples of typical fits (solid lines) to the fractal BET [30] model to nitrogen adsorption isotherms for carbon paper samples CU1 (△), CL1 (◯) and CH1 (□).

Table 1
Parameters obtained from fits of the BET [25], fractal FHH [11] and fractal BET [30] models to nitrogen adsorption data from carbon paper samples CU1, CL1, and CH1

Model	Parameter	Sample		
		CU1	CL1	CH1
BET [25]	Specific area ($m^2\ g^{-1}$)	0.81 ± 0.01	8.38 ± 0.08	5.61 ± 0.06
	Fitted P/P_0	0.08–0.21	0.08–0.21	0.08–0.21
	C	16	51	36
FHH [11]	d	2.80 ± 0.07	2.68 ± 0.03	2.56 ± 0.01
	n	2.4–16.0	1.5–7.3	1.2–6.6
	Length scale (nm)	0.8–5.6	0.5–2.6	0.4–2.3
	R^2	0.991	0.9983	0.9995
Fractal BET [30]	d	2.81 ± 0.13	2.59 ± 0.01	2.43 ± 0.004
	n	5.3–16.7	2.1–6.4	1.7–5.3
	Length scale (nm)	1.9–5.8	0.7–2.2	0.6–1.9
	R^2	0.9948	0.9999	0.9999

dimension for CL1 is higher than CH1, implying that the surface has a higher degree of roughness over the length-scales indicated. This would support the fact that the BET surface area is higher for CL1 than CH1, and infers that a lower loading of the Pt catalyst results in a greater surface area, which has implications on the catalytic activity of the electrode during its use [37].

The two-component BET model, which has been used elsewhere [32], was applied to samples CU1, CL1 and CH1. The results are shown in Table 2 and illustrate that the model is valid for all samples. For sample CU1, which is predominantly made of carbon fibres with a PTFE binder the two component constants C_1 and C_2 are 13 and 50, respectively. The determined BET constant from the original BET model was 16. The results imply that the strength of interaction between the carbon and nitrogen is more predominant than that with the binder, as the determined BET constant is closer to C_1. The same can be said for samples CL1 and CH1, with components C_1 and C_2 being the carbon substrate and Pt catalyst, respectively. The results show for both materials that C_2 is the more predominant component. It can also be seen from Table 2 that the fractal dimensions obtained agree with those seen from the other models applied, indicating the validity of the model and accuracy of the results obtained.

Table 2
The results of applying a two-component fractal BET fit, via Eq. (16), to microporous carbon paper samples CU1 (unloaded, 0 mg cm^{-2} Pt), CL1 0.39 mg cm^{-2} Pt) and CH1 (4.7 mg cm^{-2} Pt)

Sample	BET specific area ($m^2\ g^{-1}$)	C	C_1	C_2	d
CU1	0.81 ± 0.006	16	13	50	2.76 ± 0.02
CL1	8.38 ± 0.08	51	13	106	2.59 ± 0.03
CH1	5.61 ± 0.06	36	13	34	2.38 ± 0.02

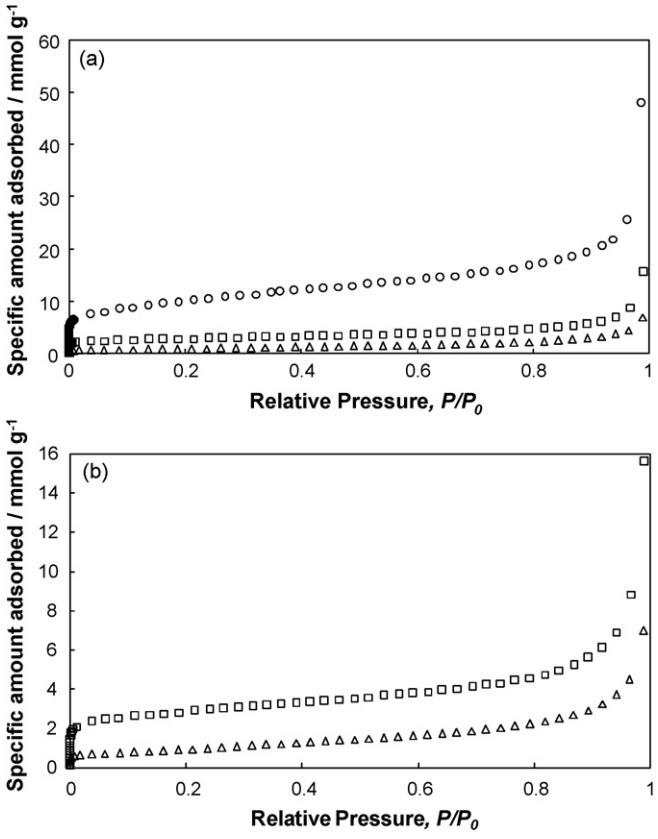

Fig. 6. (a) Nitrogen adsorption isotherms for particulate carbon support samples CP1 (◯), CP2 (□) and CP3 (△). (b) A more detailed image of samples CP2 (□) and CP3 (△).

4.2. Particulate carbon support samples CP1–CP2

Fig. 6(a) and (b) shows the isotherms for the adsorption of nitrogen on samples CP1, CP2 and CP3. It can clearly be seen that there is a significant difference in the amount adsorbed between the three samples. All samples can be classified as isotherm type II, although CP1 is indicative of a sample with high C(BET) and a large volume of micropores. Samples CP2 and CP3 show relatively similar amounts adsorbed, whereas sample CP1 adsorbed ca. 7 and 3 times as much as samples CP2 and CP3, respectively. The three samples have been analysed using the fractal FHH [11] and fractal BET [30] models. Examples of the fits are shown in Figs. 7 and 8.

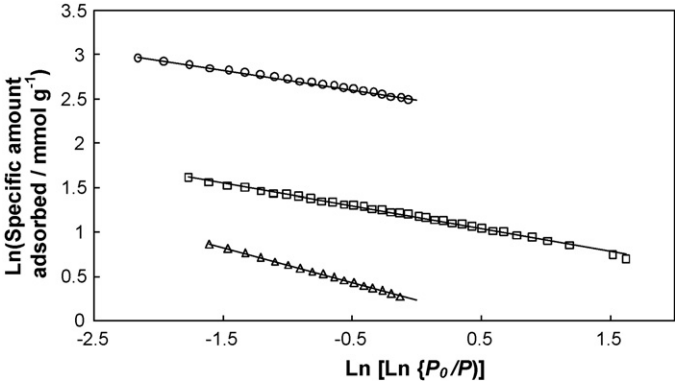

Fig. 7. Examples of typical fits (solid lines) to the fractal FHH [12] model to nitrogen adsorption isotherms for particulate carbon support samples CP1 (◯), CP2 (□) and CP3 (△).

Table 3
Parameters obtained from fits of BET [25], fractal FHH [11], fractal BET [30], fractal Porod Law [38] and DFT [39] for particulate carbon support samples CP1, CP2, and CP3

Model	Parameter	Sample		
		CP1	CP2	CP3
BET [25]	Specific surface area ($m^2\ g^{-1}$)	795.7 ± 2.2	n/a	78.4 ± 0.5
	C	204	n/a	50
	d	2.73 ± 0.07	2.74 ± 0.03	2.55 ± 0.05
FHH [11]	n	5.78–48.06	1.03–34.49	3.41–14.90
	Length scale (nm)	2.02–16.86	0.37–12.07	1.19–5.23
	R^2	0.997	0.9954	0.9996
	d	2.78 ± 0.03	–	2.6 ± 0.01
Fractal BET [30]	n	7.05 ± 46.69	–	0.89–23.94
	Length scale (nm)	2.47–16.34	–	0.31–8.38
	R^2	0.9937	–	0.9972
	d	2.76 ± 0.06	1.90 ± 0.01	2.56 ± 0.03
SAXS [38]	Ln q (nm^{-1})	−0.5 to −2.0	−0.5 to −2.0	0 to −2.0
	Length scale (nm)	0.5–2.0	0.5–2.0	0–2.0
	R^2	0.9993	0.9981	0.9986
	d	2.81 ± 0.009	1.90 ± 0.01	2.61 ± 0.01
DFT [39]	Cumulative specific surface area ($m^2\ g^{-1}$)	n/a	125.7	n/a

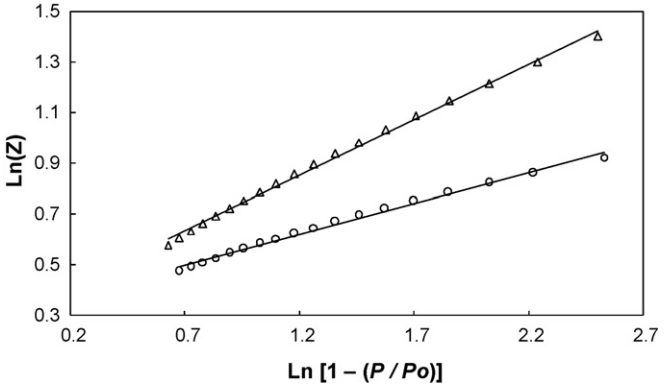

Fig. 8. Examples of typical (solid lines) fits to the fractal BET [30] model to nitrogen adsorption isotherms for particulate carbon support samples CP1 (○) and CP3 (△).

Small angle X-ray scattering data was acquired for the three samples and examples of the fits to Eq. (16) are shown in Fig. 9. Table 3 shows the parameters obtained from the fits of the sample data to the standard BET model [25], fractal FHH model [11], fractal BET model [30], and the fractal Porod Law [32]. It can be seen that the BET surface area for the three samples vary greatly, and from the high values of the surface area and C constant calculated for sample CP1, it can be inferred that the sample is microporous (average pore size <2 nm). Sample CP3 possesses a surface area that is more indicative of a mesoporous solid (average pore size 2–50 nm). Table 3 also shows that the BET model was only applied to samples CP1 and CP3. The BET model was not valid for sample CP2 and as a result, the experimental isotherm was fitted to a distribution of model isotherms calculated by density functional theory (DFT), as described elsewhere [39]. The theory assumes slit shaped pores and the fit of the model to experimental data is shown in Fig. 10. The model shows a very good fit to the experimental data, and implies that sample CP2 is comprised of micro-, meso- and macropores, according to IUPAC definitions [40].

The most striking result from the application of these models to the data is that sample CP2, which exhibited a negative C constant from the fitting of the original BET model, also resulted in a fractal dimension obtained independently by SAXS that did not match with that obtained from the fractal FHH model. The other two samples, CP1 and CP3, show extremely good agreement from the use of all the models, especially CP3 which resulted in a fractal dimension that was almost identical for all the models used. This result strongly illustrates the importance of applying various structural models/techniques to investigate the characteristics of complex carbon materials.

In addition, it has been previously shown [32] that the presence of adsorbed chemical species on the surface of porous catalysts may have a significant effect on the catalysts adsorption properties. This

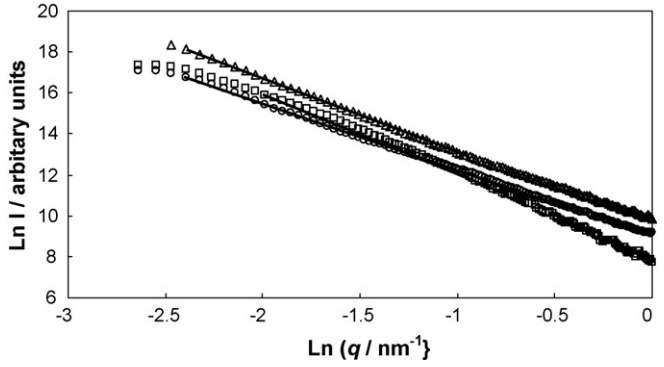

Fig. 9. Examples of typical fits (solid lines) to the fractal Porod Law [38] to the small angle X-ray scattering data for particulate carbon support samples CP1 (○), CP2 (□) and CP3 (△), according to Eq. (16).

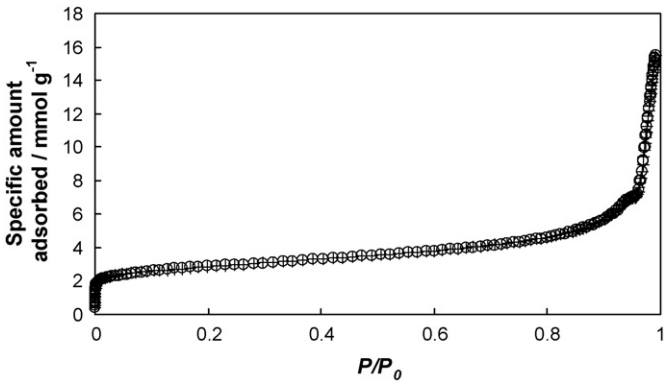

Fig. 10. Nitrogen adsorption (+) and DFT (o) isotherms for particulate carbon support sample CP2 (Vulvan XC72R).

was shown to be the case during the adsorption of nitrogen on a variety of porous silica catalyst pellets. It is possible that a similar effect occurs within sample CP2, and, as a result, an incorrect fractal dimension is obtained.

5. Conclusions

(1) The results obtained have shown that the surface structures of the three carbon paper samples (CU1, CL1 and CH1) vary significantly. Sample CU1 showed a low porosity, low surface area and is highly disordered, whereas CL1 had a high surface area (in relation to the samples examined here) and a more increased order, whilst CH1 showed a lower surface area and fractal dimension than CL1. In terms of BET surface area, it would be expected that the samples would increase in the order CU1 < CL1 < CH1. However, this was not the case, perhaps because of the large cracks present in CL1, which would result in an increased adsorbance of adsorbate. In terms of fractal dimension, the results obtained followed an identical trend to that of the BET area. If the cracks seen in CL1 were not present, the BET area would decrease, and the resultant fractal dimension would be less than that of CH1. The cracks seen in CL1 were formed due to stress experienced through the Pt layer during the deposition process.

(2) Three porous, particulate carbon blacks (CP1, CP2 and CP3) used as electrocatalyst supports for MEAs have been characterised using gas adsorption and a variety of structural models. The results have shown that sample CP1 was highly porous, whilst sample CP3 was relatively mesoporous. The fits of both samples to the fractal FHH and BET models showed very close fractal dimensions and implied that the models are valid for the materials. The fractal dimensions obtained from the two models agreed within experimental error to the fractal dimension obtained from SAXS. These results implied that the models accurately describe the surface roughness. Sample CP2, however, did not show a valid *C* constant derived from the BET model and, as a result, the fractal BET model was not valid. The surface area values calculated by DFT imply that the material was comprised of micro-, meso- and macropores.

(3) The models used were valid for samples CP1 and CP3 but not CP2 The behaviour of CP2 may be explained by the presence of chemical species on the pore surface, which may interact with the adsorptive leading to a complex surface layer. The fact that the BET model did not hold for CP2 may indicate certain restraints in the assumptions of the model, namely that the BET model assumes chemically heterogeneous surfaces. The results for samples CP1 and CP3 suggest that the models used were valid, as the results obtained from gas adsorption agree with those obtained from SAXS. This is apparent from two models with different theories applied to two different physical processes.

(4) The results obtained here can be used to provide information on the design of future PEM electrodes and MEA assemblies. By understanding the physical characteristics of existing materials, such as those examined here, in more detail, it is possible to fabricate future materials that may improve the operating performance of PEM fuel cells.

Acknowledgements

SPR, FCW and MJW-S thank the EPSRC for financial support (under grant no. GR/R61680/01). The authors are grateful to A. O'Reily for technical assistance with the scanning electron and transmission electron micrographs. Dr. D. Thompsett (Johnson Matthey Technology Centre) provided helpful comments on our early studies.

References

[1] H. Marsh, Carbon Materials: An Overview of Carbon Artifacts, in: H. Marsh, E.A. Heintz, F. Rodríguez-Reinoso (Eds.), Introduction to Carbon Technologies, Universidad de Alicante, Spain, 1997, pp. 1–33.
[2] E. Fitzer, K.H. Köchling, H.P. Boehm, H. Marsh, Pure Appl. Chem. 67 (1995) 473–506.
[3] A.L. Dicks, J. Power Sources 156 (2006) 128–141.
[4] M.B. Sweatman, N. Quirke, Langmuir 17 (2001) 5011–5020.
[5] W. Xu, T.W. Zerda, H. Raab, D. Goritz, Carbon 35 (1997) 471–474.
[6] T.W. Zerda, W. Xu, A. Zerda, Y. Zhao, R.B. Von Dreele, Carbon 38 (2000) 355–361.
[7] T. Ungár, J. Gubicza, G. Ribárik, C. Pantea, T.W. Zerda, Carbon 40 (2002) 929–937.
[8] T. Rieker, M. Hindermann-Bischoff, F. Ehrburger-Dolle, Langmuir 16 (2000) 5588–5592.
[9] E. Hoinkis, E.B.F. Lima, P. Schubert-Bischoff, Langmuir 20 (2004) 8823–8830.
[10] W. Xu, T.W. Zerda, H. Yang, M. Gerspacher, Carbon 34 (1996) 165–171.
[11] P. Pfeifer, D. Avnir, J. Chem. Phys. 79 (1983) 3371–3558.
[12] G. Halsey, J. Chem. Phys. 16 (1948) 931–937.
[13] K. Kinoshita, Carbon—Electrochemical and Physicochemical Properties, Wiley, New York, 1988, pp. 1–17.
[14] D.D. Do, H.D. Do, Carbon 41 (2003) 1777–1791.
[15] N.H. Turner, V.R. Deitz, Carbon 11 (1973) 256–258.
[16] V.J. Mimeault, D.W. McKee, Nature 224 (1969) 793–794.
[17] L.T. Drzal, J.A. Mescher, D.L. Hall, Carbon 17 (1979) 375–382.
[18] O. Tanaike, H. Hatori, Y. Yamada, S. Shiraishi, A. Oya, Carbon 41 (2003) 1759–1764.
[19] F. Nakao, Y. Takenaka, H. Asai, Composites 23 (1992) 365–372.
[20] J. Mayer, S. Giorgetta, B. Koch, E. Wintermantel, J. Patscheider, G. Spescha, Composites 25 (1994) 763–769.
[21] Y. Huang, R.J. Young, J. Mater. Sci. 29 (1994) 4027–4036.
[22] J.B. Donnet, R.Y. Qin, Carbon 31 (1993) 7–12.
[23] J. Economy, M. Daley, E.J. Hippo, D. Tandon, Carbon 33 (1995) 344–345.
[24] H. Peterlik, P. Fratzl, K. Kromp, Carbon 32 (1994) 939–945.
[25] S. Brunauer, P.H. Emmett, E. Teller, J. Am. Chem. Soc. 60 (1938) 309–319.
[26] P.H. Emmett, S. Brunauer, J. Am. Chem. Soc. 56 (1937) 35–41.
[27] K.W. Sing, F. Schüth, Handbook of Porous Solids, Wiley-VCH, Germany, 2002, pp. 84–88.
[28] P. Pfeifer, Y.J. Wu, M.W. Cole, J. Krim, Phys. Rev. Lett. 62 (1989) 1997–2000.
[29] P. Pfiefer, K.Y. Liu, Stud. Surf. Sci. Catal. 104 (1997) 625–677.
[30] M. Mahnke, H. Mögel, Colloids Surf. A 216 (2003) 215–228.
[31] J.J. Fripiat, L. Gatineau, H. van Damme, Langmuir 2 (1986) 562–567.
[32] M.J. Watt-Smith, K.J. Edler, S.P. Rigby, Langmuir 21 (2005) 2281–2292.
[33] S.C. Reyes, E. Iglesia, J. Catal. 129 (1991) 457–472.
[34] S.P. Rigby, K.J. Edler, J. Colloid Interf. Sci. 250 (2002) 175–190.
[35] P. Debeye, H.R. Anderson, H. Brumberger, J. Appl. Phys. 28 (1957) 679–683.
[36] L. Larminie, A. Dicks, Fuel Cell Systems Explained, 2nd ed., John Wiley & Sons, England, 2003, pp. 72–75.
[37] M.J. Watt-Smith, The Characterisation of Porous Catalysts using Magnetic Resonance Imaging and other Experimental Techniques, Ph.D. Thesis, University of Bath, UK, 2006.
[38] K.W. Sing, F. Schüth, Handbook of Porous Solids, Wiley-VCH, Germany, 2002, pp. 145–150.
[39] J.P. Olivier, J. Porous Mater. 2 (1995) 9–17.
[40] J. Rouquerol, D. Avnir, C.W. Fairbridge, D.H. Everett, J.H. Haynes, N. Pernicone, J.D.F. Ramsay, K.S.W. Sing, K.K. Unger, Pure Appl. Chem. 66 (1994) 1739–1758.